

Robust Kernel-based Feature Representation for 3D Point Cloud Analysis via Circular Convolutional Network

Seunghwan Jung, Yeong-Gil Shin, and Minyoung Chung*

Abstract—Feature descriptors of point clouds are used in several applications, such as registration and part segmentation of 3D point clouds. Learning representations of local geometric features is unquestionably the most important task for accurate point cloud analyses. However, it is challenging to develop rotation or scale-invariant descriptors. Most previous studies have either ignored rotations or empirically studied optimal scale parameters, which hinders the applicability of the methods for real-world datasets. In this paper, we present a new local feature description method that is robust to rotation and scale variations. Moreover, we improved representations based on a global aggregation method. First, we place kernels aligned around each point in the normal direction. To avoid the sign problem of the normal vector, we use a symmetric kernel point distribution in the tangential plane. From each kernel point, we first projected the points from the spatial space to the feature space, which is robust to multiple scales and rotation, based on angles and distances. Subsequently, we perform convolutions by considering local kernel point structures and long-range global context, obtained by a global aggregation method. We experimented with our proposed descriptors on benchmark datasets (i.e., ModelNet40 and ShapeNetPart) to evaluate the performance of registration, classification, and part segmentation on 3D point clouds. Our method showed superior performances when compared to the state-of-the-art methods by reducing 70% of the rotation and translation errors in the registration task. Our method also showed comparable performance in the classification and part-segmentation tasks without any external data augmentation.

Index Terms—Angle-based kernel convolutions, global context aggregation, rotation-robust point descriptor, scale adaptation, 3D point cloud analysis.



1 INTRODUCTION

POINT cloud analysis is becoming a popular research area owing to the growth in the capability of 3D sensors to capture rich geometric 3D information. The applications of point cloud analysis include robotics, autonomous driving, and augmented/mixed reality. Extracting salient local geometric information is a fundamental task for analyzing point clouds to match correspondences between two objects [1] or to analyze the geometric information [2]. Recently, end-to-end learning based on point or graph convolutional networks has outperformed earlier works, which were primarily developed using hand-crafted feature descriptors [3] [4]. However, building rotation- or scale-invariant descriptors remains a difficult task in the field of computer vision research.

Descriptors of point cloud applications have been widely researched for point cloud registration, model segmentation, and classification. PointNet [5] shows a new paradigm for point cloud analysis by introducing a permutation-invariant method; however, it is difficult to encode the local geometric information. The point pair feature network (PPFNet) [6] encodes local features by employing PointNet [5] for local regions and a deep graph convolutional neural network

(DGCNN) [2] encodes the relative position of neighbors for each point. However, these methods are limited to extracting rotation-invariant features. In practice, it must be noted that the point cloud is not aligned to the same frame, indicating that random rotation of the input point cloud can significantly affect the representation of the descriptors. Kernel point convolution (KPConv) [7] uses kernel points around each point to efficiently handle irregularly distributed point clouds. KPConv has demonstrated groundbreaking performance; however, this rotation-variant descriptor limits the performance for randomly rotated objects, which are obtained by multiview scans. 3DSmoothNet [1] extracts local region points and aligns the local points to the local reference frame of the center point. The primary limitation of 3DSmoothNet is that the sign of a normal axis and the directions of the other two axes are not unique in a planar region. Descriptors that are aligned by an inaccurate local reference frame may encode different geometric contexts. In the example of point cloud registration, if the corresponding points have different normal signs, descriptors from the points may hamper the identification of correspondences. Moreover, local descriptors only encode local geometric information, which results in difficulty in encoding the global geometry. Consequently, local descriptors of monotonous and repeating areas are typically considered to be nonsalient descriptors, which indicates that global registration can be mismatched.

To overcome this limitation, we propose a rotation- and scale-robust descriptor-generation method. Inspired by

*Asterisk indicates corresponding author.
(This paper is under consideration at Computer Vision and Image Understanding.)*

S. Jung and Y.-G. Shin are with the Department of Computer Science and Engineering, Seoul National University, South Korea.

**M. Chung is with the School of Software, Soongsil University, South Korea (e-mail: chungmy@ssu.ac.kr).*

KPConv [7] and 3DSmoothNet [1], our proposed method aligns the kernels to the normal vector and extracts rotation-robust features. Owing to the nonuniqueness of the local reference frame in the planar region, we distributed kernels in the form of a cylindrical shape. This shape is symmetrical around a tangent plane to handle the sign problem and has a circular cross section to handle the other undefined reference axes. By employing this kernel structure, we applied convolution with adjacent kernels combined together such that the descriptor is not affected by rotation. To make the descriptor robust to the scale of the local frame, we analyzed the geometric information and rebuilt the descriptor with a modified kernel size. In addition, to improve representations of the descriptor from the monotonous and repeating areas, we aggregated all features based on the distances from each point to encode discriminative global features.

The major contributions of this work can be summarized as follows:

- The rotation-robust descriptor is developed based on the kernel alignment.
- The sign problem, which is caused by the normal direction of the vector, is resolved by the proposed angle-based convolution.
- The scale factor, which is derived from the size of a kernel, is automatically defined for each point using a scale adaptation module.
- Global context is effectively extracted by the proposed aggregation method with each local context.

We analyzed the working of our proposed method on three types of tasks: registration, classification, and part segmentation. We trained and tested our proposed method on ModelNet40 dataset [8] for classification and registration and on ShapeNet dataset [9] for segmentation.

The remainder of this paper is organized as follows. In Section II, several hand-crafted and deep-learning-based 3D features are reviewed. The proposed method is described in Section III. The experimental results, discussion, and conclusion are presented in Sections IV, V, and VI, respectively.

2 RELATED WORKS

2.1 Hand-crafted 3D features

Before the advance of deep learning, a 3D feature descriptor was developed based on hand-crafted methods. Local descriptors were generated based on the relationship between a point and the spatial neighborhoods around the point. In addition, certain methods built a rotation-invariant descriptor based on a local reference frame. Spin-images [10] align neighbors using the surface normal of the interest point and represent aligned neighbors to the cylindrical support region using radial and elevation coordinates. The 3D Shape Context descriptor [11] represents neighbors in the support region with grid bins divided along the azimuth, elevation, and radial values. The Unique Shape Context method [12] extends the 3D Shape Context method by applying a local reference frame based on the covariance matrix. Similarly, the signature of histograms of orientations algorithm [3] also calculates the local reference frame and builds a histogram using angles between point normal vectors. Point feature histograms [13] and fast point feature histograms [4] select

neighbors for each point and build a histogram using pairwise geometric differences between neighbors and the point of interest, such as relative distance and angles. Recently, with the advent of deep neural networks for point cloud data (e.g., PointNet [5] and DGCNN [2]), feature descriptors have shown groundbreaking results when compared to hand-crafted methods in several vision tasks.

2.2 Deep learning based 3D features

2.2.1 Volumetric based Methods

The conversion of the point cloud to a volumetric data representation has been widely used to employ grid-based convolutions [14], [15]. However, the quantification of the floating-point data results in an approximation, such that the input data intrinsically contains discretized artifacts. Because the voxelization process severely consumes memory, these methods typically approximate the input data into a coarse grid of volumetric representation. To overcome this problem, certain methods represent point cloud data by optimizing the memory consumption. OctNet [16] divides the space by employing a set of unbalanced octrees based on density. Certain methods use a sparse tensor that only saves the nonempty space coordinates and features [17], [18], [19].

To build a rotation-invariant descriptor, 3DSmoothNet [1] was used to calculate the local reference frame based on the covariance of points and to transform neighbor points within the spherical support area of the interest point using the local reference frame before voxelizing the points. However, the sign of a normal axis and the directions of the other two axes are not unique in the planar region. Descriptors that are aligned using an inaccurate local reference frame may encode different geometric contexts. Therefore, we assume that the sign of the normal vector is not unique and uses a customized kernel similar to the KPConv [7] method to overcome the sign issue. SpinNet [20] aligned each point and neighbors of the point (i.e., patch) with the z-axis and mapped the point patch to the cylindrical volume to build rotation-invariant descriptors. However, since the method used the volumetric-based method for each point patch, it required a lot of computational memory to build descriptors. Moreover, since each volume contained only one point patch, the user has to determine the optimal patch size to be trained (i.e., fixed scale). On the contrary, our proposed method consumed a relatively small amount of computational memory when compared to SpinNet [20] and automatically determined the kernel size using the scale adaptation module.

2.2.2 Point based Methods

PointNet [5] and PointNet++ [21] are pioneering works for point cloud analysis, which are based on deep neural networks. These methods encode unstructured point clouds using a shared multilayer perceptron and build a permutation-invariant descriptor using a global max-pooling layer. Based on PointNet, various methods have been developed to improve performance. PPFNet [6] extended PointNet [5] to learn local geometric features. PPFNet built local features by employing PointNet and subsequently fused global information based on the local features by employing max-pooling. PPF-FoldNet [22] used rotation-invariant features

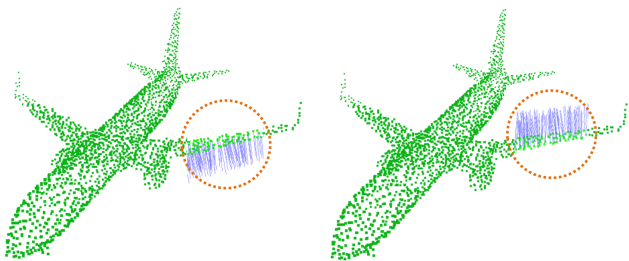


Fig. 1: Visualization of normal vectors. The signs for each point on a planar surface are not determined uniquely.

such as angles and distances between the interest point and its neighbor and trained the descriptor by using folding-based auto-encoding in an unsupervised fashion. DGCNN [2] selected k -nearest neighbors for each point and encoded the relative locations of the neighbors to encapsulate the geometric information. ShellNet [23] partitioned the neighbors of each point into shells based on the distances from the point to resolve the point order ambiguity. KPConv [7] proposed a kernel-based point convolution method that placed kernel points around each point to effectively handle irregularly distributed point clouds, and further, aggregated the geometric information from the kernel points. We extended the KPConv method by employing normal kernel alignment and angle-based convolution. As described in KPConv, a normal vector is available for artificial data [7]. In the real-world dataset, a local reference frame is inaccurate because of the sign problem (i.e., the uncertain direction of the normal vector; Fig. 1). To overcome the inaccuracy of the local reference frame, we aligned the kernels and extracted features based on the unsigned normal axis, and subsequently applied convolution operations that are invariant to the sign problem. Various rotation-invariant methods have been studied based on the rotation-invariant features, such as relative distance, angle [24] [25], and quaternion [26]. RIF [27] represented neighbors of the interest point by using rotation-invariant features and constructed a point relation matrix to supplement insufficient global information. The method showed better performances when compared to the other methods under rotations, but showed inferior performances under non-rotation environments when compared to non-rotation-invariant methods. It is challenging to develop a rotation-robust descriptor with a good benchmark accuracy because of two reasons: 1) It is hard to represent the accurate relationship between points with rotation-invariant features. 2) Convolution with more than one point in rotation-invariant-order is a challenging problem. In that aspect, our proposed method represented neighbors with not only the rotation-invariant features, but the kernels to supplement the relationship representation. Further, we used the circular convolution method, which processed the adjacent kernels simultaneously to capture the relationships between the points.

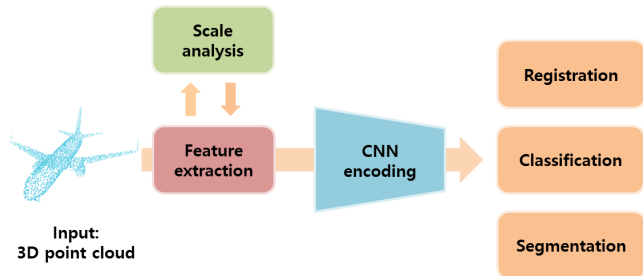


Fig. 2: Overview of the proposed architecture. First, features are extracted using multiple kernel sizes. Subsequently, scale analysis is employed based on the interpolation between the kernel sizes. Finally, the feature descriptor is encoded using the adjusted scale for the downstream tasks.

3 METHOD

Figure 2 illustrates an overview of the proposed descriptor-generation framework. The point descriptor is built by using information obtained from the kernels around the point. To build rotation-invariant kernels, we use the normal vectors of each point to align the kernels (Section A). Local information is extracted from the kernels to encode the feature descriptors (Section B). Subsequently, circular convolution is applied, which is invariant to the sign problem (Section C). A scale adaptation module is employed in the network to resolve the scale issues (Section D). Various convolutional neural network (CNN) encoder architectures are presented in Section E, which were used for downstream tasks in this study. Finally, the global context estimation is demonstrated, which is employed in the encoder architectures (Section F).

3.1 Kernel alignment

To build a rotation-robust descriptor, we aligned the kernels around each point using the local reference axis, i.e., normal vector. Inspired by the 3DsmoothNet [1], we estimated the normal vector using the eigenvector of the neighbor point covariance matrix. However, the sign of the normal vector and the remaining local reference axes are not unique if a point is located on a planar surface. To resolve these ambiguities, we used cylinder-shaped kernels in which the cylinder column is aligned to the normal vector.

Figure 3(a) illustrates the kernel distribution. The cross section of the cylinder is a circle along the normal direction. We placed the kernels for each circle (i.e., four to six numbers of kernels), and grouped them as one layer. In total, we used three layers for the cylinder (i.e., additional upper and lower regions of the tangent plane).

3.2 Rotation robust feature projection

Once all the kernels are aligned for each point, the k -nearest neighbor points from each kernel are extracted. The averaged location is then calculated based on their distance from the kernel:

$$\hat{x}_i^k = \sum_{x_j \in N(x_i^k)} \frac{w_j x_j}{\sum w_j} \text{ where } w_j = \exp\left(\frac{-(x_j - x_i^k)^2}{d^2}\right), \quad (1)$$

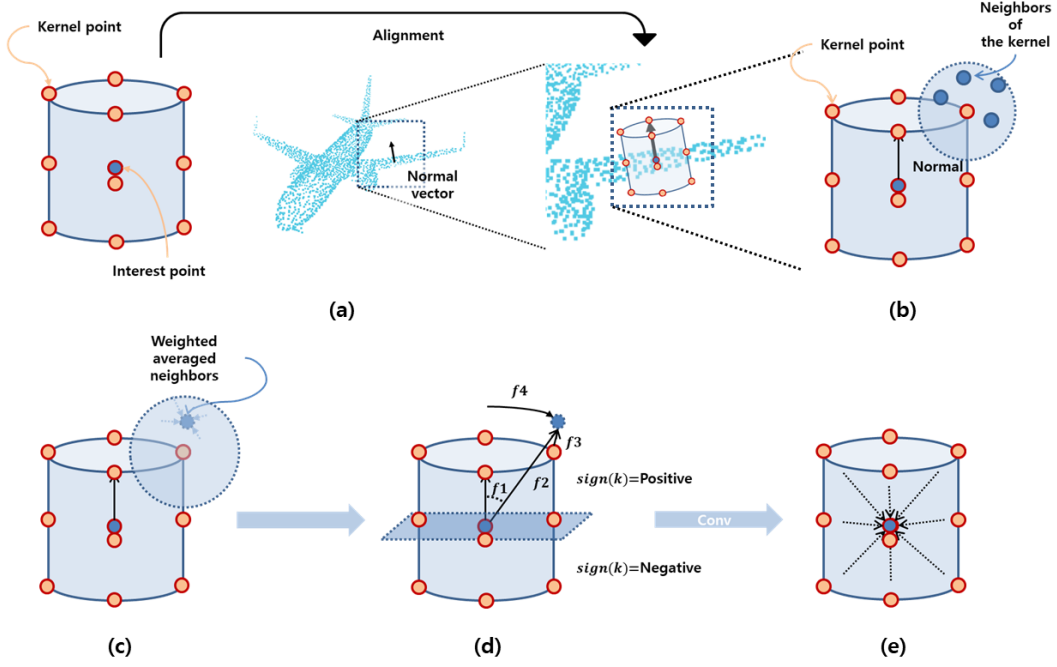


Fig. 3: (a) Kernel points are aligned using the normal vector of the target point; (b) Neighbors are selected for each kernel point; (c) Weighted-average location is estimated based on the distance from the kernel point to the neighbors; (d) For each kernel, the relative location of the averaged neighbor is estimated using distances and angles; (e) After convolution, kernel features are aggregated by summation and maximum value selection to represent the interest point.

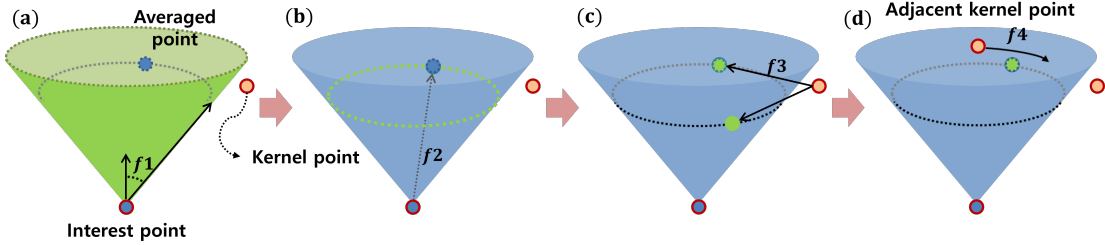


Fig. 4: Candidates of the neighbor points corresponding to extracted features. Green regions of (a), (b), (c), and (d) illustrate the candidates corresponding to the features $(f1)$, $(f1, f2)$, $(f1, f2, f3)$, and $(f1, f2, f3, f4)$, respectively.

where $\hat{x}_i^k \in \mathbb{R}^{N \times 3}$ is the weighted-average location of the k -th kernel point of x_i and d indicates the distance from the center point to the kernel point. For the weighting term, i.e., w_j we used the Gaussian function to reduce the influence of outliers in (1).

For rotation-robust representations, we estimated four types of features. We first estimated the angles between two vectors: one is from the center point of the kernels to the weighted-average point and the other is the normal vector (the angle $f1$ in Fig. 3(d)). However, because the normal vector has a normal orientation problem (i.e., sign ambiguity), a negative sign is multiplied with the normal vector if the kernel is located below the tangent plane, as shown below:

$$f1_i^k = v_i \cdot \frac{\hat{x}_i^k - x_i}{\|\hat{x}_i^k - x_i\|} \cdot \text{sign}(k) \quad (2)$$

where v_i indicates the normal vector of x_i and $\text{sign}(k)$ returns a negative sign if the kernel is located below the tangent plane. This term determines the angle value, regardless of the normal sign.

Next, we estimated the distances from the point to the averaged neighbors and from the center of the kernels to the averaged neighbors (distances $f2$ and $f3$ in Fig. 3(d)):

$$f2_i^k = \left\| \frac{\hat{x}_i^k - x_i}{d} \right\| \quad (3)$$

$$f3_i^k = \left\| \frac{\hat{x}_i^k - x_i^k}{d} \right\| \quad (4)$$

To provide direction to the closest adjacent kernel points, we estimated the distance ratio from two adjacent kernel points

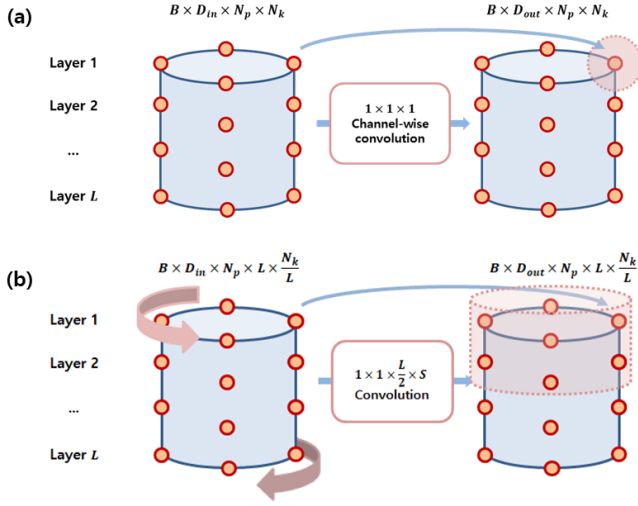


Fig. 5: (a) Channel-wise convolution and (b) circular convolution. The red transparent region indicates the receptive field. S indicates the kernel size of the convolution.

to the averaged point (ratio f_4 in Fig. 3(d)):

$$f_4^k = \frac{\|\hat{x}_i^k - x_i^{k+1}\|}{\|\hat{x}_i^k - x_i^{k+1}\| + \|\hat{x}_i^k - x_i^{k-1}\|} \quad (5)$$

The relative location of the averaged neighbor points can be successfully encoded based on the presented angle- and distance-based descriptions. Figure 3 illustrates the entire process of feature extraction, and figure 4 illustrates candidates of the neighbor points corresponding to extracted features. By using our features, we can represent the relative positions of neighbors accurately.

3.3 Circular convolution

Because the kernels are not aligned to the unique local reference frames, the order of the kernels may change depending on the point distribution. However, the adjacent kernels within the cylinder layer are invariant to rotation. Therefore, we extended $1 \times 1 \times 1$ channel-wise convolution based on (6) to (7):

$$x_i = \sum_{\hat{x}_i^k} f(g(\hat{x}_i^k)), \quad (6)$$

$$x_i = \sum_{\hat{x}_i^k} f(g(\hat{x}_i^{c(k,-1)}), g(\hat{x}_i^k), g(\hat{x}_i^{c(k,+1)})), \quad (7)$$

where $c(k,+1)$ and $c(k,-1)$ indicate the clockwise and counterclockwise adjacent kernels of the k -th kernel in the cylinder layer. Subsequently, to avoid the sign problem, kernels are divided into two groups: the collection of kernels above the tangent plane and the collection of kernels below the tangent plane. If the kernel belongs to the first group, we select the clockwise adjacent kernel in a clockwise order. Otherwise, we select the kernel in a counterclockwise order.

In addition, we processed convolution with multiple layers if the layers belong to the same group, i.e., (7) is extended to

$$x_i = \sum_{\hat{x}_i^k} f(g(\hat{x}_i^k), g(\hat{x}_i^j)_{j \in adj(k)}), \quad (8)$$

where $adj(k)$ indicates a set of adjacent kernel points of the k -th kernel point in the same group. A circular padding convolution operation was used to implement (8). Figure 5 illustrates the convolution process using the kernels. After convolution, the kernel features around the interest point are aggregated by the summation and maximum value selection.

3.4 Scale adaptation module

If a target object has an unusual shape when compared to the training data, the normalization process might fail to resolve the scale problem. Because performing normalization cannot resolve the scale problem completely, we first normalized the target objects, and subsequently performed the scale adaptation module on the normalized objects to supplement scale-robustness.

To develop a scale-robust descriptor, we adjusted the kernel size based on an analysis of the multiscaled features (d in (1)). We first extracted multiple features using multiple kernel sizes (feature extraction in Fig. 2). Subsequently, we concatenated the multiscaled features and estimated the interpolation weights between the kernel sizes. Simple convolution operations were employed for the scale analysis, as illustrated in Fig. 2. Finally, the output size of the kernel was used to encode the proposed descriptor for CNN encoding (Fig. 2).

3.5 CNN encoder architectures

The designed CNN encoders are illustrated in Fig. 6. For the registration task, four feature-extraction layers are initially used. Using a shortcut connection, the multiscale features are concatenated. Subsequently, global contexts from the concatenated features are estimated to improve the representations (as described in the following subsection, Section F). Inspired by the deep closest point (DCP) method [28], the singular value decomposition (SVD) module is used to estimate the transformation matrix. For the classification and segmentation tasks, we used the downsampling and upsampling operations which reduces and increase the number of points by using subsampling. Subsequently, Additional fully connected layers (multi-layered perceptron) are used to estimate the scores.

3.6 Aggregating global context

Local descriptors of monotonous and repeating areas are typically considered as nonsalient descriptors. To improve representations of the descriptor, we estimated the global context from local features (global context module in Fig. 6). Rather than estimating a single global context for all points using max-pooling, we estimated the adaptive global contexts for each point by using distance-based weights.

To estimate the global feature for the i -th point, weights w_{ij} are calculated based on the Gaussian distance between

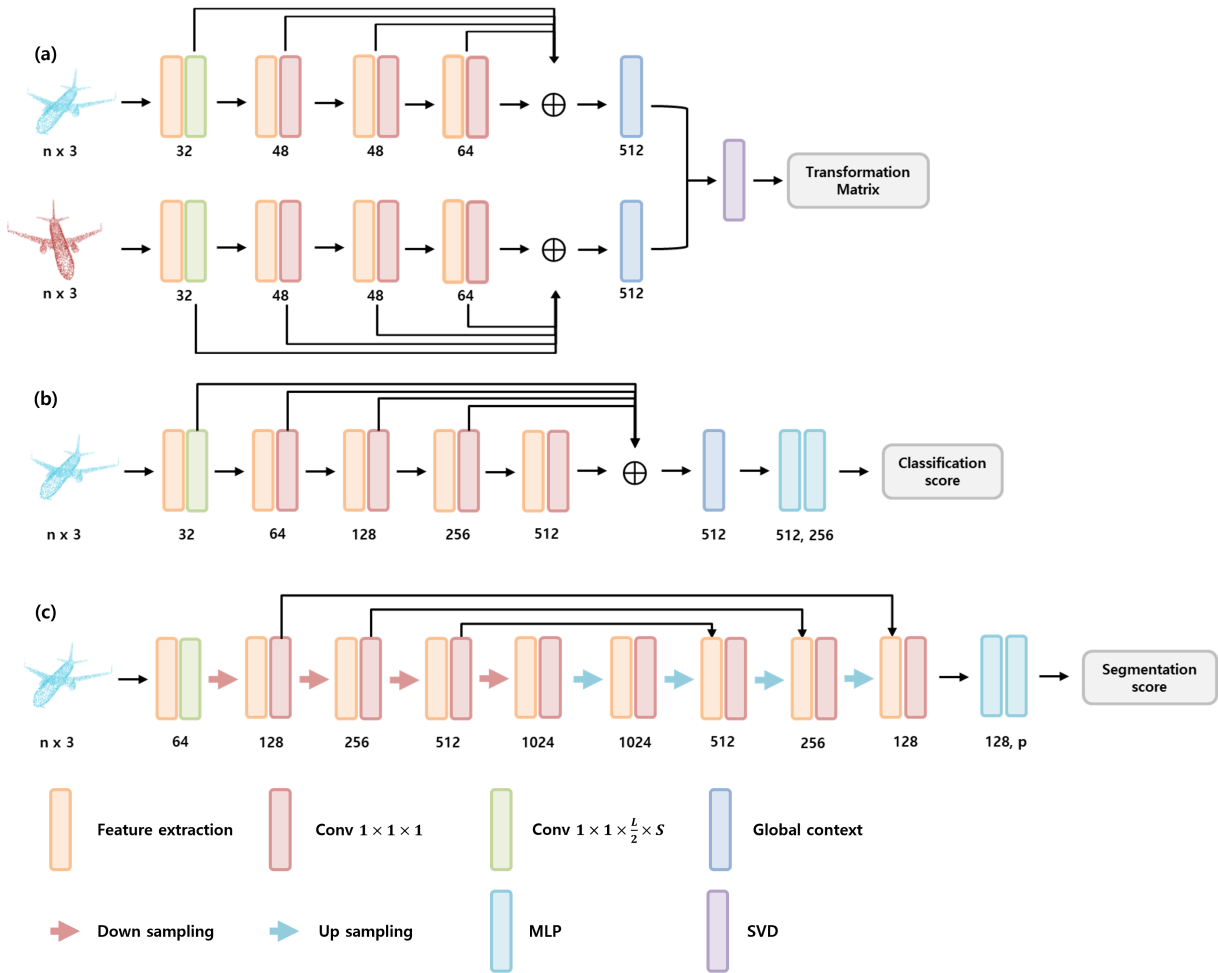


Fig. 6: Network architectures for (a) registration, (b) classification, and (c) part segmentation.

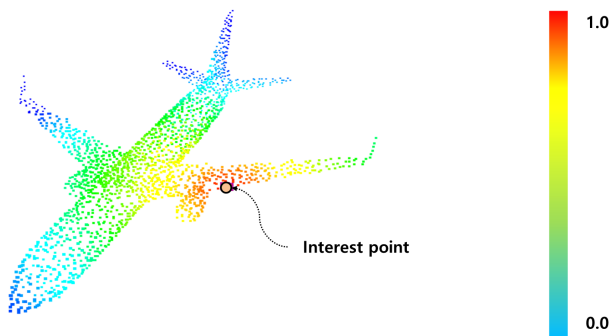


Fig. 7: Colors of point cloud indicate global context weights of the interest point. Red indicates a weight value of one and blue indicates a weight value of zero.

the i -th and j -th points (weights for an interest point in Fig. 7). Subsequently, the averaged local features are estimated using the weights w_{ij} for all j .

$$g_i = \sum \frac{w_{ij} f_j}{\sum w_{ij}} \text{ where } w_{ij} = \exp\left(\frac{-(x_j - x_i)^2}{d^2}\right) \quad (9)$$

Once the global contexts are estimated for each point, the

global contexts are concatenated to each local feature. Finally, a convolution operation is performed on concatenated features.

4 RESULT

We implemented three tasks: registration, classification, and segmentation. For the registration and classification tasks, we used the ModelNet40 database [8]. For the segmentation task, we used the ShapeNetPart database [9]. For the registration task, we compared our methods with PointNetLK [29] and DCP [28]. In the case of classification and part-segmentation tasks, we compared our methods with several methods, such as PointNet [5], DGCNN [2], and KPConv [7].

We analyzed our method on the registration task using the ModelNet40 database [8]. ModelNet40 contains 12,311 meshed computer-aided design models from 40 categories. ModelNet40 is split by category into training and test sets; the first 20 categories among the 40 categories were used for training. For each model, 1,024 points were used for training and testing.

The DCP method [28] presented an end-to-end network for a rigid registration. Inspired by this method, we used the SVD module to compute a rigid transformation. Figure 6(a)

illustrates the registration architecture. As evaluation metrics, the mean squared error, root mean squared error, and mean absolute error were used for rotation and translation.

4.1 Registration

As listed in Table 1, our method significantly reduced the registration errors when compared to the other methods since the methods used translation-invariant features, not rotation-invariant features. Even when compared to the results trained with all categories, our method showed better performance.

We conducted the partial registration task by using the sampled point clouds from ModelNet40 inspired by PRNet [32]. The overall architecture is similar to the registration architecture. One difference is that we computed a rigid transformation using a RANSAC [53] with the generated descriptors. Table 2 lists the partial registration results. SpinNet [20] aligned and mapped the point patch to the cylindrical volume to capture detailed geometric information. Subsequently, the method used the continuous convolution method to capture the geometric structure in a rotation-invariance manner. However, there are three drawbacks: 1) Severe memory consumption, 2) the optimal patch size, and 3) the sign problem. On the contrary, our proposed method consumed relatively a small amount of computational memory when compared to SpinNet [20] and automatically determined the kernel size using the scale adaptation module. Moreover, our method concerned the sign problem by using the symmetric circular convolution method. As a result, our method significantly reduced the registration errors with simple architecture and less computation memory.

Figure 8 illustrates the registration results of the DCP [28] and proposed methods. The results of the DCP method [28] showed a small error between the two point clouds. Conversely, the results of our method showed superior matching performance. These results indicate that the proposed descriptor matches the feature-based correspondences between the source and target points in a superior manner when compared to the DCP [28].

4.2 Classification and Segmentation

We analyzed the classification and part-segmentation performances of our method using ModelNet40 [8] and ShapeNetPart [9] databases, respectively. ModelNet40 contains 12,311 models. Among the models, 9,843 models were used for training, and the remaining 2,468 models were used for testing. For each model, 1,024 points were used for training and testing. ShapeNetPart contains 16,681 models from 16 categories. Each point is annotated using part labels. For each model, we used 2,048 points for training and testing.

Figures 6(b) and (c) illustrate the classification and part-segmentation architectures, respectively. Table 3 lists the classification and part-segmentation results. While considering the evaluation metrics, the overall accuracy was used for ModelNet40 classification and mean intersection over union was used for ShapeNetPart segmentation. We compared our methods with the non-rotation-invariant methods and rotation-invariant methods. The non-rotation-invariant methods typically represented the relationship

between points based on point coordinates. Unlike the non-rotation-invariant methods, the rotation-invariant methods used rotation-invariant features (e.g. relative distance and angle) to achieve rotation-invariant property. However, it is hard to represent the accurate relationship between points with rotation-invariant features, and convolution with more than one point in rotation-invariant-order is a challenging problem. Therefore, as listed in Table 3, the non-rotation-invariant methods showed better performances when compared to the rotation-invariant methods under non-rotation environments.

To address the problems, our proposed method represented neighbors with not only the rotation-invariant features, but the kernels to supplement the relationship representation. Further, we used the circular convolution method, which processed the adjacent kernels simultaneously to capture the relationships between the points. Therefore, as clearly demonstrated in Table 3, our proposed descriptor outperformed the rotation-invariant methods and achieved comparable performance when compared to the non-rotation-invariant methods. Because the non-rotation-invariant methods typically used point coordinates as the features, it was easy to learn geometric information based on each point location. On the contrary, to develop a rotation-robust descriptor, we used rotation-invariant features. Moreover, we aligned our kernels to the normal vector, and it means that the order of the kernels may change depending on the point distribution unlike the non-rotation-invariant methods. These properties affected the method performance, and thus our method showed inferior performances when compared to the state-of-the-art non-rotation-invariant methods under non-rotation environments. However, rotation-invariance is a desired feature for real-world applications. Thus, it is significant that our proposed method achieved superior accuracy among the rotation-invariant methods.

4.3 Parameter and ablation study

We conducted several parameter and ablation studies on the registration task to verify the effect of our method (Table 4), i.e., by varying the following parameters: convolution operation, the number of nearest neighbors for each kernel, and global context.

First, we experimented with the convolution methods, i.e., $1 \times 1 \times 1$ channel-wise convolution and circular convolution methods. The network with circular convolution significantly improved the performance in terms of both rotation and translation. These results indicate that the circular convolution operations successfully captured the geometric features based on adjacent kernels. Figure 9 illustrates the registration results according to the kernel alignment and convolution methods. As illustrated, the network with the aligned kernel-based circular convolution showed better registration results.

Second, we analyzed our method with a different number of neighbors. As listed in Table 4, the errors were not significantly dependent on the number of neighbors. Because we used the distance-based weights for each neighbor, the closer neighbors had more influence. Owing to the use of the distance-based weights, employing the averaged neighbors reduced the influence of the number of neighbors.

Method	R-MSE	R-RMSE	R-MAE	T-MSE	T-RMSE	T-MAE	C
ICP	892.601	29.876	23.626	0.086	0.293	0.251	-
Go-ICP [30]	192.258	13.865	2.914	0.000	0.022	0.006	-
FGR [31]	97.002	9.848	1.445	0.000	0.013	0.002	-
PointNetLK [29]	306.323	17.502	5.280	0.000	0.028	0.007	20
PointNetLK [29]	227.870	15.095	4.225	0.000	0.022	0.005	40
DCP-v2 [28]	9.923	3.150	2.007	0.000	0.005	0.003	20
DCP-v2 [28]	1.307	1.143	0.770	0.000	0.001	0.001	40
Our method	0.017	0.130	0.064	0.000	0.000	0.000	20

TABLE 1: Global registration results for ModelNet40. The evaluation metrics are mean squared error (MSE), root mean squared error (RMSE), and mean absolute error (MAE) for rotation (R-) and translation (T-). C indicates the number of categories for training.

Method	R-MSE	R-RMSE	R-MAE	T-MSE	T-RMSE	T-MAE
ICP	297.080	17.236	8.610	0.007	0.082	0.043
Go-ICP [30]	184.199	13.572	3.416	0.002	0.045	0.015
FGR [31]	40.832	6.390	1.240	0.001	0.038	0.008
PointNetLK [29]	334.67	18.294	9.730	0.008	0.092	0.053
DCP [28]	45.617	6.754	4.366	0.004	0.061	0.040
PRNet [32]	7.355	2.712	1.372	0.000	0.017	0.012
FMR [33]	25.412	5.041	2.304	0.001	0.038	0.016
IDAM [34]	46.950	6.852	1.761	0.003	0.054	0.014
DeepGMR [35]	356.832	18.890	9.322	0.008	0.087	0.056
OMNet [36]	4.322	2.079	0.619	0.000	0.018	0.008
SpinNet [20]	1.355	1.164	0.902	0.000	0.013	0.011
Our method	0.741	0.861	0.440	0.000	0.008	0.004

TABLE 2: Partial registration results for ModelNet40.

Method	OA	mIoU	mcIoU	RI
SPLATNet [37]	-	85.4	83.7	X
SGPN [38]	-	85.8	82.8	X
3DmFV-Net [39]	91.6	84.3	81.0	X
SynSpecCNN [40]	-	84.7	82.0	X
RSNet [41]	-	84.9	81.4	X
SpecGCN [42]	91.5	85.4	-	X
PointNet [5]	89.2	83.7	80.3	X
PointNet++ [21]	90.7	85.1	81.9	X
KD-Net [43]	90.6	82.3	77.4	X
SO-Net [44]	90.9	84.9	81.0	X
PCNN by Ext [45]	92.3	85.1	81.8	X
SpiderCNN [46]	90.5	85.3	82.4	X
MCCConv [47]	90.9	85.9	-	X
FlexConv [48]	90.2	85.0	84.7	X
PointCNN [49]	92.2	86.1	84.6	X
DGCNN [2]	92.2	85.2	85.0	X
SubSparseCNN [39]	-	86.0	83.3	X
KPConv [7]	92.9	86.2	85.1	X
ShellNet [23]	93.1	-	-	X
Point Transformer [50]	93.7	86.6	83.7	X
PACConv [51]	93.9	86.1	84.6	X
RI-ShellConv [24]	86.5	80.3	75.3	O
ClusterNet [25]	87.1	-	-	O
REQNN [26]	83.0	-	-	O
PRIN [52]	-	71.1	67.6	O
RIF [27]	89.4	82.5	79.4	O
Our method	93.2	85.9	83.3	O

TABLE 3: ModelNet40 classification results (i.e. OA) and ShapeNetPart segmentation results (i.e. mIoU). OA, mIoU, and mcIoU indicate the overall accuracy, instance average intersection over union, and class average intersection over union, respectively. RI indicates whether the method is the rotation-robust method or not.

Third, we conducted registration with the global context. Consequently, the rotation error decreased significantly when compared to the other experiments. These results demonstrate that the global context resolves the ambiguities of each local descriptor.

4.4 Robustness study

In addition to the parameter studies on the registration task, we conducted scale- and rotation- robust studies for evaluation. First, we experimented with the scale adaptation module. The network is trained with the original scale (1.00) of point clouds and tested with different scales (0.50, 1.50) to demonstrate the scale robustness. Table 5 lists the results of different scale tests for each model. The mean and standard deviations are presented, and the proposed network showed stable results when the network used the scale adaptation module. The results indicate that the scale adaptation module determined the optimal kernel size to capture geometric information so that the performance of the global registration outperformed.

In addition, to demonstrate the rotation robustness, we trained the network with azimuthal rotations (around the gravity axis) (ZR) and arbitrary rotations (AR) and tested with arbitrary rotations (ZR/AR, AR/AR) for the classification and segmentation (Table 6 and 7). (-/-) indicates which rotational metric was used for training/testing, respectively.

We compared the results with state-of-the-art rotation-invariant methods to demonstrate the rotation robustness. The rotation-invariant methods [24] [25] used rotation-invariant features to represent the relative positions of neighbors and processed each point using MLP to avoid processing in non-rotation-invariant order. However, since there is no additional reference point, the used rotation-

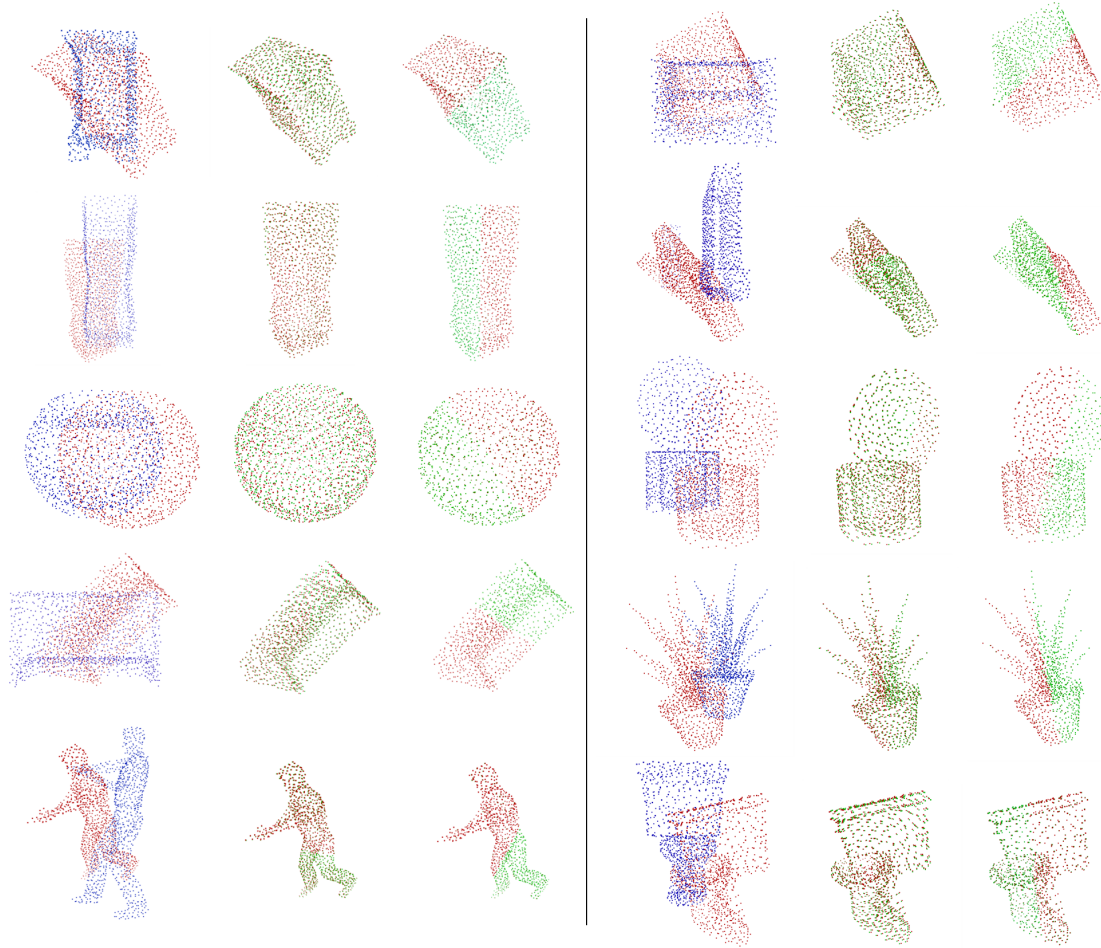


Fig. 8: Left: source (blue) and target (red) point clouds, Middle: registration results of deep closest point method [28]. Green indicates the transformed source point clouds. Right: registration results of our method.

invariant features were insufficient to completely represent the relative positions [24] [25]. RIF [27] used the additional reference points, but the reference points have a chance to be changed depending on object shape variation, and it may result in insufficient consistency of the descriptors between similar object parts. Moreover, the shared MLP simply processed each point feature without considering other points.

On the contrary, by using the kernels (i.e., reference points) which have fixed distances from an interest point, our proposed method can represent the relative positions of neighbors accurately. Moreover, by using the circular convolution method which processed the adjacent kernels at once

to capture the relationships between the information, our descriptor improved geometric information representations.

As a result, in the case of training and evaluating under arbitrary rotation (AR/AR), our method showed superior performances when compared to the state-of-art methods. In addition, in the case of training under azimuthal rotation and evaluating under arbitrary rotation (ZR/AR), the accuracy losses of our methods were not significant when compared to the other non-rotation-invariant methods since our method used rotation-invariant features.

Conv method	R-MSE	R-RMSE	R-MAE	T-MSE	T-RMSE	T-MAE
channel-wise	0.040420	0.201046	0.105576	0.000000	0.000149	0.000094
circular conv	0.017159	0.130991	0.064475	0.000000	0.000048	0.000027
KNN	R-MSE	R-RMSE	R-MAE	T-MSE	T-RMSE	T-MAE
10	0.017159	0.130991	0.064475	0.000000	0.000048	0.000027
2	0.014517	0.120486	0.065029	0.000000	0.000037	0.000025
Global information	R-MSE	R-RMSE	R-MAE	T-MSE	T-RMSE	T-MAE
X	0.017159	0.130991	0.064475	0.000000	0.000048	0.000027
O	0.008142	0.091766	0.046526	0.000000	0.000047	0.000027

TABLE 4: Parameter and ablation study for ModelNet40 global registration task.

Scale adaptation (training/test scale)	R-MSE	R-RMSE	R-MAE	T-MSE	T-RMSE	T-MAE
X (1.00/0.50)	0.111988	0.334647	0.112045	0.000000	0.000044	0.000031
X (1.00/1.00)	0.017159	0.130991	0.064475	0.000000	0.000048	0.000027
X (1.00/1.50)	0.023768	0.154168	0.080950	0.000000	0.000150	0.000082
X (Total)	0.050971 \pm 0.043229	0.206601 \pm 0.0910345	0.085823 \pm 0.019723	0.000000 \pm 0.000000	0.000080 \pm 0.000049	0.000046 \pm 0.000025
O (1.00/0.50)	0.041671	0.204134	0.073383	0.000000	0.000056	0.000036
O (1.00/1.00)	0.021910	0.148021	0.055841	0.000000	0.000039	0.000025
O (1.00/1.50)	0.027835	0.166837	0.064757	0.000000	0.000073	0.000046
O (Total)	0.030472 \pm 0.008280	0.172997 \pm 0.023318	0.064660 \pm 0.007161	0.000000 \pm 0.000000	0.000056 \pm 0.000013	0.000035 \pm 0.000008

TABLE 5: ModelNet40 global registration results with different scales. (1.0/#) is the experiments in which networks are trained with the original scale of point clouds and tested with (#) scale of point clouds. Values indicate the mean and standard deviation of the results.

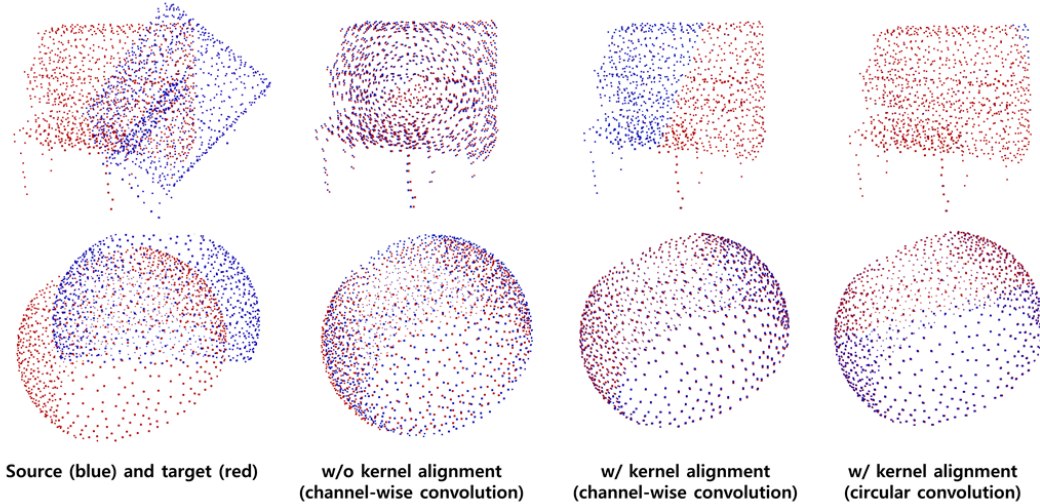


Fig. 9: Comparison of methods

Method	OA (ZR/AR)	OA (AR/AR)	RI
PointNet [5]	16.4	75.5	X
PointNet++ [21]	28.6	85.0	X
PointCNN [49]	41.2	84.5	X
DGCNN [2]	20.6	81.1	X
ShellNet [23]	19.9	87.8	X
KPConv [7]	47.8	87.8	X
RI-ShellConv [24]	86.5	86.5	O
ClusterNet [25]	87.1	87.1	O
REQNN [26]	83.0	-	O
RIF [27]	89.4	89.3	O
Our method	89.0	91.0	O

TABLE 6: Classification results with rotations for ModelNet40. ZR and AR indicate the azimuthal rotations (ZR) and arbitrary rotations (AR), respectively.

5 DISCUSSION

Point cloud analysis requires rotation- and scale-robust feature representation. It is challenging to develop a robust descriptor with a good benchmark accuracy. In this paper, we propose an aligned kernel-based feature representation to resolve these limitations. To make the descriptor robust to rotation, we aligned the kernels to the local reference frame. Subsequently, we applied normal sign-independent convolutions to the descriptors rather than using fixed kernels that are independent of the rotations [7]. Instead of

Method	mIoU (ZR/AR)	mIoU (AR/AR)	RI
PointNet [5]	37.8	74.4	X
PointNet++ [21]	48.3	76.7	X
PointCNN [49]	34.7	71.4	X
DGCNN [2]	37.4	73.3	X
ShellNet [23]	47.2	77.1	X
KPConv [7]	46.3	75.8	X
RI-ShellConv [24]	75.3	75.3	O
PRIN [52]	64.6	67.6	O
RIF [27]	79.2	79.4	O
Our method	73.7	80.1	O

TABLE 7: Results of ShapeNetPart segmentation. mIoU indicates the class average intersection over union. The second and third column (i.e., ZR/AR and AR/AR) indicate values of mIoU obtained from training the data based on ZR and AR, respectively, and tested on AR.

using translation-invariant features [2], we used rotation-robust features from the aligned kernels. In addition, to improve the representations of the descriptor, we estimated the adaptive global context for each point rather than using a single global context [6]. Because the kernel-based descriptors are highly dependent on the size of the given kernels, we adjusted the kernel size based on the trainable weights.

The experimental results for various tasks (i.e., registration, classification, and part segmentation) showed promis-

ing results for feature representation. In the registration task, the rotation and translation errors decreased significantly. This indicates that our descriptors successfully captured the salient and corresponding geometric information between the two transformed point clouds. In the case of classification and segmentation tasks, our proposed method showed the best performances under rotations. These results indicate that our method is not only limited to the transformed point cloud task but also applicable to general purposes (i.e., feature representations). Several parameter and ablation studies have also demonstrated that our proposed methods improved the feature representations and stability of the descriptor.

6 CONCLUSION

Encoding rotation- and scale-robust features is a challenging task for point cloud representation. The robustness of each parameter is critical for a successful application in various downstream tasks. In this paper, we proposed a CNN-based feature encoding method to resolve this task. The proposed kernel alignment, feature projection, and kernel-conscious convolution methods demonstrated superior performance on the registration task when compared to previous methods. Moreover, the proposed scale adaptation and global aggregation methods successfully captured the optimum scale parameter and global geometric features for each local descriptor, respectively.

REFERENCES

- [1] Z. Gojcic, C. Zhou, J. D. Wegner, and A. Wieser, "The perfect match: 3d point cloud matching with smoothed densities," in *2019 IEEE/CVF Conference on Computer Vision and Pattern Recognition (CVPR)*, 2019, pp. 5540–5549.
- [2] A. V. Phan, M. L. Nguyen, Y. L. H. Nguyen, and L. T. Bui, "Dgcn: A convolutional neural network over large-scale labeled graphs," *Neural Networks*, vol. 108, pp. 533–543, 2018. [Online]. Available: <http://www.sciencedirect.com/science/article/pii/S0893608018302636>
- [3] S. Salti, F. Tombari, and L. Di Stefano, "Shot: Unique signatures of histograms for surface and texture description," *Computer Vision and Image Understanding*, vol. 125, 08 2014.
- [4] R. B. Rusu, N. Blodow, and M. Beetz, "Fast point feature histograms (fpfh) for 3d registration," in *2009 IEEE International Conference on Robotics and Automation*, 2009, pp. 3212–3217.
- [5] R. Q. Charles, H. Su, M. Kaichun, and L. J. Guibas, "Pointnet: Deep learning on point sets for 3d classification and segmentation," in *2017 IEEE Conference on Computer Vision and Pattern Recognition (CVPR)*, 2017, pp. 77–85.
- [6] H. Deng, T. Birdal, and S. Ilic, "Ppfnet: Global context aware local features for robust 3d point matching," in *2018 IEEE/CVF Conference on Computer Vision and Pattern Recognition*, 2018, pp. 195–205.
- [7] H. Thomas, C. R. Qi, J. Deschaud, B. Marcotegui, F. Goulette, and L. Guibas, "Kpconv: Flexible and deformable convolution for point clouds," in *2019 IEEE/CVF International Conference on Computer Vision (ICCV)*, 2019, pp. 6410–6419.
- [8] Zhirong Wu, S. Song, A. Khosla, Fisher Yu, Linguang Zhang, Xiaoou Tang, and J. Xiao, "3d shapenets: A deep representation for volumetric shapes," in *2015 IEEE Conference on Computer Vision and Pattern Recognition (CVPR)*, 2015, pp. 1912–1920.
- [9] L. Yi, V. G. Kim, D. Ceylan, I. Shen, M. Yan, H. Su, C. Lu, Q. Huang, A. Sheffer, and L. Guibas, "A scalable active framework for region annotation in 3d shape collections," *ACM Transactions on Graphics (TOG)*, vol. 35, pp. 1–12, 2016.
- [10] A. E. Johnson and M. Hebert, "Using spin images for efficient object recognition in cluttered 3d scenes," *IEEE Transactions on Pattern Analysis and Machine Intelligence*, vol. 21, no. 5, pp. 433–449, 1999.
- [11] A. Frome, D. Huber, R. Kolluri, T. Bülow, and J. Malik, "Recognizing objects in range data using regional point descriptors," vol. 3, 05 2004, pp. 224–237.
- [12] F. Tombari, S. Salti, and L. Di Stefano, "Unique shape context for 3d data description," 01 2010.
- [13] R. Rusu, N. Blodow, Z. Marton, and M. Beetz, "Aligning point cloud views using persistent feature histograms," 09 2008, pp. 3384–3391.
- [14] D. Maturana and S. Scherer, "Voxnet: A 3d convolutional neural network for real-time object recognition," in *2015 IEEE/RSJ International Conference on Intelligent Robots and Systems (IROS)*, 2015, pp. 922–928.
- [15] C. Ruizhongtai Qi, H. Su, M. NieBner, A. Dai, M. Yan, and L. Guibas, "Volumetric and multi-view cnns for object classification on 3d data," 06 2016, pp. 5648–5656.
- [16] G. Riegler, A. O. Ulusoy, and A. Geiger, "Octnet: Learning deep 3d representations at high resolutions," in *2017 IEEE Conference on Computer Vision and Pattern Recognition (CVPR)*, 2017, pp. 6620–6629.
- [17] B. Graham, "Spatially-sparse convolutional neural networks," 2014.
- [18] C. Choy, J. Gwak, and S. Savarese, "4d spatio-temporal convnets: Minkowski convolutional neural networks," 06 2019, pp. 3070–3079.
- [19] C. Choy, J. Park, and V. Koltun, "Fully convolutional geometric features," in *2019 IEEE/CVF International Conference on Computer Vision (ICCV)*, 2019, pp. 8957–8965.
- [20] S. Ao, Q. Hu, B. Yang, A. Markham, and Y. Guo, "Spinnet: Learning a general surface descriptor for 3d point cloud registration," in *Proceedings of the IEEE/CVF Conference on Computer Vision and Pattern Recognition*, 2021, pp. 11753–11762.
- [21] C. R. Qi, L. Yi, H. Su, and L. J. Guibas, "Pointnet++: Deep hierarchical feature learning on point sets in a metric space," in *Advances in Neural Information Processing Systems 30: Annual Conference on Neural Information Processing Systems 2017, 4-9 December 2017, Long Beach, CA, USA*, I. Guyon, U. von Luxburg, S. Bengio, H. M. Wallach, R. Fergus, S. V. N. Vishwanathan, and R. Garnett, Eds., 2017, pp. 5099–5108. [Online]. Available: <http://papers.nips.cc/paper/7095-pointnet-deep-hierarchical-feature-learning-on-point-sets-in-a-metric-space>
- [22] H. Deng, T. Birdal, and S. Ilic, "Ppf-foldnet: Unsupervised learning of rotation invariant 3d local descriptors," in *ECCV*, 2018.
- [23] Z. Zhang, B.-S. Hua, and S.-K. Yeung, "Shellnet: Efficient point cloud convolutional neural networks using concentric shells statistics," in *Proceedings of the IEEE/CVF International Conference on Computer Vision*, 2019, pp. 1607–1616.
- [24] Z. Zhang, B.-S. Hua, D. W. Rosen, and S.-K. Yeung, "Rotation invariant convolutions for 3d point clouds deep learning," in *2019 International Conference on 3D Vision (3DV)*. IEEE, 2019, pp. 204–213.
- [25] C. Chen, G. Li, R. Xu, T. Chen, M. Wang, and L. Lin, "Cluster-net: Deep hierarchical cluster network with rigorously rotation-invariant representation for point cloud analysis," in *Proceedings of the IEEE/CVF Conference on Computer Vision and Pattern Recognition*, 2019, pp. 4994–5002.
- [26] W. Shen, B. Zhang, S. Huang, Z. Wei, and Q. Zhang, "3d-rotation-equivariant quaternion neural networks," in *Computer Vision—ECCV 2020: 16th European Conference, Glasgow, UK, August 23–28, 2020, Proceedings, Part XX 16*. Springer, 2020, pp. 531–547.
- [27] X. Li, R. Li, G. Chen, C.-W. Fu, D. Cohen-Or, and P. Heng, "A rotation-invariant framework for deep point cloud analysis," *IEEE transactions on visualization and computer graphics*, vol. PP, 2021.
- [28] Y. Wang and J. Solomon, "Deep closest point: Learning representations for point cloud registration," 10 2019, pp. 3522–3531.
- [29] Y. Aoki, H. Goforth, R. A. Srivatsan, and S. Lucey, "Pointnetlk: Robust efficient point cloud registration using pointnet," in *2019 IEEE/CVF Conference on Computer Vision and Pattern Recognition (CVPR)*, 2019, pp. 7156–7165.
- [30] J. Yang, H. Li, D. Campbell, and Y. Jia, "Go-icp: A globally optimal solution to 3d icp point-set registration," *IEEE Transactions on Pattern Analysis and Machine Intelligence*, vol. 38, no. 11, pp. 2241–2254, 2016.
- [31] Q.-Y. Zhou, J. Park, and V. Koltun, *Fast Global Registration*, 2016, pp. 766–782. [Online]. Available: <https://app.dimensions.ai/details/publication/pub.1034541096>
- [32] Y. Wang and J. Solomon, "Prnet: Self-supervised learning for partial-to-partial registration," in *NeurIPS*, 2019.

- [33] X. Huang, G. Mei, and J. Zhang, "Feature-metric registration: A fast semi-supervised approach for robust point cloud registration without correspondences," in *Proceedings of the IEEE/CVF Conference on Computer Vision and Pattern Recognition*, 2020, pp. 11 366–11 374.
- [34] J. Li, C. Zhang, Z. Xu, H. Zhou, and C. Zhang, "Iterative distance-aware similarity matrix convolution with mutual-supervised point elimination for efficient point cloud registration," in *European conference on computer vision*. Springer, 2020, pp. 378–394.
- [35] W. Yuan, B. Eckart, K. Kim, V. Jampani, D. Fox, and J. Kautz, "Deepgmr: Learning latent gaussian mixture models for registration," in *European conference on computer vision*. Springer, 2020, pp. 733–750.
- [36] H. Xu, S. Liu, G. Wang, G. Liu, and B. Zeng, "Omnet: Learning overlapping mask for partial-to-partial point cloud registration," in *Proceedings of the IEEE/CVF International Conference on Computer Vision*, 2021, pp. 3132–3141.
- [37] H. Su, V. Jampani, D. Sun, S. Maji, E. Kalogerakis, M.-H. Yang, and J. Kautz, "Splatnet: Sparse lattice networks for point cloud processing," 06 2018, pp. 2530–2539.
- [38] W. Wang, R. Yu, Q. Huang, and U. Neumann, "Sgpn: Similarity group proposal network for 3d point cloud instance segmentation," in *2018 IEEE/CVF Conference on Computer Vision and Pattern Recognition*, 2018, pp. 2569–2578.
- [39] B. Graham, M. Engelcke, and L. v. d. Maaten, "3d semantic segmentation with submanifold sparse convolutional networks," in *2018 IEEE/CVF Conference on Computer Vision and Pattern Recognition*, 2018, pp. 9224–9232.
- [40] L. Yi, H. Su, X. Guo, and L. Guibas, "Syncspecnn: Synchronized spectral cnn for 3d shape segmentation," in *2017 IEEE Conference on Computer Vision and Pattern Recognition (CVPR)*, 2017, pp. 6584–6592.
- [41] Q. Huang, W. Wang, and U. Neumann, "Recurrent slice networks for 3d segmentation of point clouds," in *2018 IEEE/CVF Conference on Computer Vision and Pattern Recognition*, 2018, pp. 2626–2635.
- [42] C. Wang, B. Samari, and K. Siddiqi, *Local Spectral Graph Convolution for Point Set Feature Learning: 15th European Conference, Munich, Germany, September 8-14, 2018, Proceedings, Part IV*, 09 2018, pp. 56–71.
- [43] R. Klokov and V. Lempitsky, "Escape from cells: Deep kd-networks for the recognition of 3d point cloud models," in *2017 IEEE International Conference on Computer Vision (ICCV)*, 2017, pp. 863–872.
- [44] J. Li, B. M. Chen, and G. H. Lee, "So-net: Self-organizing network for point cloud analysis," in *2018 IEEE/CVF Conference on Computer Vision and Pattern Recognition*, 2018, pp. 9397–9406.
- [45] M. Atzmon, H. Maron, and Y. Lipman, "Point convolutional neural networks by extension operators," *ACM Trans. Graph.*, vol. 37, no. 4, Jul. 2018. [Online]. Available: <https://doi.org/10.1145/3197517.3201301>
- [46] Y. Xu, T. Fan, M. Xu, L. Zeng, and Y. Qiao, "Spidernn: Deep learning on point sets with parameterized convolutional filters," 03 2018.
- [47] P. Hermosilla, T. Ritschel, P.-P. Vazquez Alcocer, A. Vinacua, and T. Ropinski, "Monte carlo convolution for learning on non-uniformly sampled point clouds," vol. 37, 12 2018, pp. 1–12.
- [48] F. Groh, P. Wieschollek, and H. Lensch, *Flex-Convolution: Million-Scale Point-Cloud Learning Beyond Grid-Worlds*, 05 2019, pp. 105–122.
- [49] Y. Li, R. Bu, M. Sun, W. Wu, X. Di, and B. Chen, "Pointcnn: Convolution on x-transformed points," in *NeurIPS*, 2018.
- [50] H. Zhao, L. Jiang, J. Jia, P. H. Torr, and V. Koltun, "Point transformer," in *Proceedings of the IEEE/CVF International Conference on Computer Vision*, 2021, pp. 16 259–16 268.
- [51] M. Xu, R. Ding, H. Zhao, and X. Qi, "Paconv: Position adaptive convolution with dynamic kernel assembling on point clouds," in *Proceedings of the IEEE/CVF Conference on Computer Vision and Pattern Recognition*, 2021, pp. 3173–3182.
- [52] Y. You, Y. Lou, Q. Liu, Y.-W. Tai, L. Ma, C. Lu, and W. Wang, "Pointwise rotation-invariant network with adaptive sampling and 3d spherical voxel convolution," in *Proceedings of the AAAI Conference on Artificial Intelligence*, vol. 34, no. 07, 2020, pp. 12 717–12 724.
- [53] M. A. Fischler and R. C. Bolles, "Random sample consensus: a paradigm for model fitting with applications to image analysis and automated cartography," *Communications of the ACM*, vol. 24, no. 6, pp. 381–395, 1981.